Plasticizer blending improved regenerated cellulose films as an alternative to plastics

Pauliina Ahokas*, Vesa Kunnari, Johanna Majoinen, Ali Harlin, Mikko Mäkelä

VTT Technical Research Centre of Finland Ltd., PO Box 1000, 02044 VTT Espoo, Finland

*Corresponding author, e-mail: pauliina.ahokas@vtt.fi

Abstract

Plasticizers are widely used to improve the elasticity of regenerated cellulose films, but academic research has thus far ignored the possibility of plasticizer blending. We studied the effects of glycerol, sorbitol, and maltitol on film properties based on a systematic design for mixture experiments and determined regression models to correlate blend composition with film properties. Our results showed that plasticizer blending enabled us to control film tensile strength and water vapour and oxygen permeabilities, which are key indicators to evaluate film efficacy in barrier packaging applications. Our films showed lower water vapor and oxygen permeabilities than commercial uncoated cellophane film and could potentially provide a renewable alternative to conventional polyolefin films with further improvements. These results are important and they indicate that plasticizer blending provides a novel and simple methodology to improve regenerated cellulose films to meet the increasing demand for alternatives to conventional plastics in packaging and other applications.

Keywords: *cellulose films, crystallinity, mixture design, permeability, regression modelling, tensile strength*

Table of contents entry

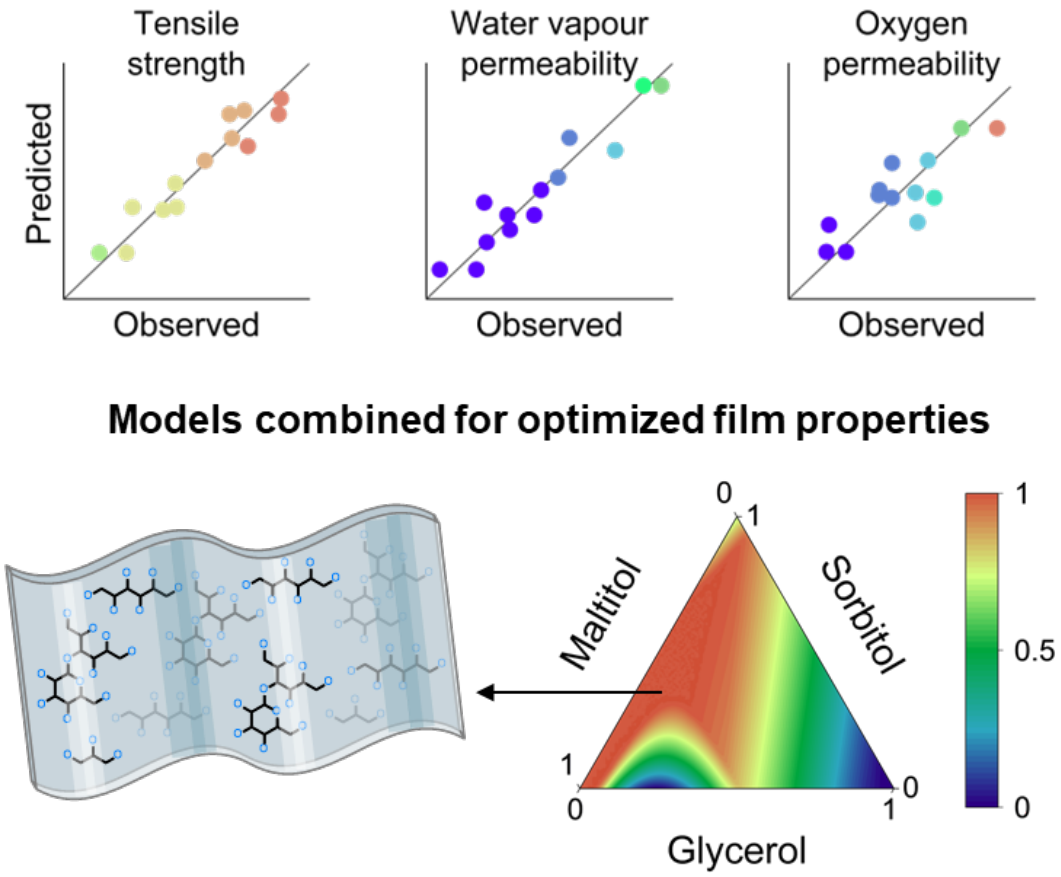

1. Introduction

Petroleum-based plastics and plastic films are widely used in packaging applications. The global production of plastics increased to 460 million tonnes in 2019 and 31% of these plastics were used for packaging (OECD, 2024a). An important application for plastics in the packaging segment is barrier packaging. Flexible barrier films, for example, are generally produced from low-density polyethylene or polypropylene with excellent moisture barrier and chemical resistance properties to ensure satisfactory shelf-life in food packaging applications. Both of these plastic types have typically low barrier performance against oxygen and carbon dioxide, which can be improved by adding polyvinyl alcohol, ethylene vinyl alcohol, polyvinylidene chloride, or aluminum oxide coatings as additional layers (Hirvikorpi et al., 2010; Mokwena and Tang, 2012; Struller et al., 2014). None of these common alternatives are, however, biodegradable and they are often difficult to recycle. Multilayer films for fresh food packaging can contain up to seven individual layers and are particularly difficult to recycle when they contain halogenated compounds, metal foils, or metallized films as functional layers (de Mello Soares et al., 2022; Ragaert et al., 2017). Recycling reduces waste generated by the packaging industry, which has an average product lifetime of 0.5 years from production to disposal compared to the 5 and 35 years of the textile and construction industries, respectively (Geyer et al., 2017). In 2019 low-density polyethylene and polypropylene from packaging formed 20% of plastic waste, which is projected to reach 1.014 billion tonnes by 2060 (OECD, 2024b). Only 17% of these wastes are estimated to be recycled, the rest will be incinerated, landfilled, or mismanaged (OECD, 2024c). These challenges have been acknowledged by the European Commission, which proposed further changes to the Directive 94/62/EC on packaging and packaging waste in 2022 aiming to prevent waste and to ensure that all packaging is cost-effectively reusable or recyclable by 2030 (Ragonnaud, 2023).

Regenerated cellulose films can provide an alternative to petroleum-based plastics in barrier packaging. Cellulose is not naturally thermoplastic but can be regenerated into different forms, such as thin films or coatings, through dissolution and precipitation. Dissolution breaks down the supramolecular structure of native cellulose I and precipitation reorients the scattered polymer chains in opposite directions to form the regenerated cellulose II polymorph (Kolpak and Blackwell, 1976). Several dissolution and precipitation chemistries have been introduced in the past century. Xanthation and alkali dissolution is used to produce viscose yarn, which is the largest regenerated cellulose application with a 90% market share (Singh et al., 2015). Xanthation is, however, connected to serious environmental and occupational risks due to the use of carbon disulphide and the formation of sulphur-containing by-products (Klemm et al., 2005). A promising alternative is to mechanically modify cellulose while pretreating it with enzymes. Moist dissolved pulp can be exposed to a tailored enzyme-cocktail and ground to improve enzyme accessibility by increasing fiber porosity (Grönqvist et al., 2014). This mechano-enzymatic pretreatment decreases the degree of polymerization of cellulose and increases porosity, which both improve dissolution into aqueous sodium zincate solution (Grönqvist et al., 2015, 2014; Vehviläinen et al., 2020, 2015).

Enzymatic mechanical pre-treatment and sodium zincate dissolution can be used to modify cellulose into biodegradable films for packaging applications. Regenerated cellulose films, however, have generally low elasticity and low-to-moderate barrier properties against water vapour and oxygen. Mechanical film properties are commonly improved with plasticizers, which are usually low molecular weight compounds used to increase film elasticity. Phthalates, for example, are plasticizers used in food casings and personal care items primarily prepared from synthetic polymers despite the increasing information on their negative impacts to human health (Lee and Choi, 2024; Vessa et al., 2022). Studies on alternative bio-based plasticizers have mainly focused on epoxidized oils, cellulose derivates, and polyols such as glycerol and its derivatives (Jin et al., 2011; Peng et al., 2021; Rebelo et al., 2023; Xiao et al., 2003). Considerably fewer studies have combined different plasticizers

(Cazón et al., 2020; de Britto et al., 2012; Sanyang et al., 2015; Zhang et al., 2023) and we found no academic studies focusing specifically on plasticizer blending.

Our objective was to improve the properties of regenerated cellulose films by focusing on plasticizer blending. We hypothesized that blending low molecular weight polyols with different number of hydroxyl groups could enable us to control the mechanical and barrier properties of cellulose films based on blend composition. Our hypothesis was based on the work of Fernández-Santos et al. (2021) who reported that the barrier properties of nanocellulose films improved with an increasing number of hydroxyl groups in the plasticizer. Thus, we studied the effects of glycerol, sorbitol, and maltitol on film properties using a systematic design for mixture experiments and determined regression models to correlate blend composition with film properties. We focused specifically on tensile strength and water vapour and oxygen permeabilities as they are considered key indicators of film efficacy for barrier applications (Fernández-Santos et al., 2021; Moreira et al., 2024). Our results are important to understand the effects of plasticizers on film properties and to develop new plasticizer blending strategies to improve film performance. These developments can improve the competitiveness of regenerated cellulose films against their petroleum-based counterparts in packaging and other applications.

2. Experimental

2.1 Design of experiments

The plasticizer experiments were designed according to a simplex centroid design originally reported by Scheffe (1963). The original mixture design was augmented with additional axial points, which contained blends of all three plasticizers (see Fig. 2a). These experiments were added to improve the predictive ability of the experiments specifically for ternary mixtures. We also replicated the glycerol, sorbitol, and maltitol experiments, which generated 13 plasticizer blend experiments (Table A1 in the Appendix). Non-plasticized cellulose films were used as control samples.

2.2 Film preparation and characterization

Dissolving grade softwood sulphite pulp purchased from Domsjö Fabriker AB was used for preparing the films. The pulp was disintegrated in deionized water and spin-dried to 33 wt.% dry matter content. The spin-dried pulp was then pretreated by enzymatic twin-screw extrusion. An enzyme mixture FiberCare R purchased from Novozymes was added to the pulp while feeding it through a twin-screw extruder for 1.5 mins. The pulp was left to age and the enzymes were inactivated by immersing the pulp in aqueous NaOH (pH 11). The pre-treated pulp was dissolved in sodium zincate by a two-stage direct dissolution procedure. The obtained dissolved cellulose solution was an aqueous mixture of 6.7 wt.% pulp, 8 wt.% NaOH and 1.6 wt.% ZnO. This solution was deaerated at 120 mbar overnight and casted on glass plates. The cast films were precipitated in an aqueous solution of 10 wt.% H_2SO_4 and 10 wt.% Na_2SO_4 and washed with tap water. Visually homogeneous films were then plasticized in an aqueous solution of 5 wt.% of the plasticizers for 60 sec. The plasticized films were dried on jigs to prevent shrinkage. All films were conditioned at 23 °C and 50% relative humidity for at least 24 hours before further analysis.

Tensile properties of the films were determined with a Lloyd LS5 testing instrument (AMETEK measurement and calibration technologies, USA) using a 100 N load cell. The films were cut into 15 mm x 80 mm long strips and at least six different film strips were measured for each experiment. The initial gauge length was 50 mm and gauges were pulled apart with an extension rate of 5 $mm \cdot min^{-1}$. Young's modulus was defined as the stress-strain slope >80% of the two-point slope maxima. Water vapour permeation was measured with PERMA-TRAN-W 3/34 analyzer (AMETEK MOCON, USA). Oxygen permeation was measured with an OX-TRAN 2/22H Permeation Analyzer (AMETEK MOCON, USA). For both WVP and OP measurements the temperature was set at 23 °C in 50% relative humidity using a cell area of 5 cm^2.

Wide-angle X-ray scattering (WAXS) spectra were recorded with a Xenocs Xeuss 3.0 SAXS/WAXS system (Xenocs SAS, Grenoble, France). The system included a microfocus X-ray source (sealed tube, operating at 50 kV and 0.6 mA) with a Cu target and a multilayer mirror yielding a parallel beam with a nominal wavelength of 1.542 Å (combined Cu K-α1 and Cu K-α2 characteristic radiation). The beam size at the sample was set to 0.4 mm. A kapton film was used as a sample holder and it's scattering signal was normalized and deducted from the measurement data. An area detector (Eiger2 R 1M, Dectris AG, Switzerland) recorded the data. The distance between the sample and the detector was calibrated by measuring the diffraction of a known standard sample LaB6. Total crystallinity index was determined based on the maximum peak intensities of the main crystalline planes (I_{110}) at around 20° and the minima (I_{AM}) between the 1-10 and 110 peaks at around 16° (Azubuike et al., 2012; Nam et al., 2016; Park et al., 2010) according to the method developed by Segal et al., (1959), Eq. (1):

$$\text{Total crystallinity index} = \left(\frac{I_{200\,OR\,110} - I_{AM}}{I_{200\,OR\,110}}\right) \quad (1)$$

Crystallite size (τ) of the main crystalline plane I_{110} at around 20° was calculated by using the Scherrer equation (French and Santiago Cintrón, 2013; Scherrer, 1918), Eq. (2):

$$\tau = \frac{\lambda K}{\beta \cos\theta} \quad (2)$$

where K denoted a crystal shape dependent constant (French and Santiago Cintrón, 2013), λ the X-ray wavelength of the incident beam in the diffraction experiment (0.1542), β the full peak width at half of its maximum, and θ the Bragg's angle, i.e., the position of the peak. Full peak width at half of its maximum was determined with non-linear Gaussian curve fitting in OriginPro 2024 (OriginLab Corp.).

2.3 Empirical models

Correlations across plasticizer composition and film properties were determined with principal components analysis. The data were compiled in a matrix and the matrix columns were normalized to unit variance and zero mean to compare variables given in different units. Correlations across the normalized variables were evaluated with the principal component loadings based on the general model equation, Eq. (3):

$$\mathbf{X} = \sum_{\mathbf{i=1}}^{\mathbf{n}} \mathbf{t}^{\mathbf{T}}\mathbf{p} + \mathbf{E_n} \quad (3)$$

where **X** denoted the normalized and mean centered data matrix, **t** denoted the orthogonal score vectors, **p** the orthonormal loadings vectors, and $\mathbf{E_n}$ a residual matrix after *n* components. The first loadings vector was determined as the set of weights that maximized the variation explained by the corresponding scores (Bro and Smilde, 2014), Eq. (4):

$$\arg\max_{\|w\|=1} (\mathbf{t}^{\mathbf{T}}\mathbf{t}) \quad (4)$$

where **w** denoted the component weights, and the loadings of subsequent principal components were set to be orthogonal to the previous ones. The principal components thus formed a new coordinate system that described the main correlations across plasticizer blend composition and film properties.

Plasticizer composition was then used to estimate individual film properties with multiple linear regression. Tensile strength and water vapour and oxygen permeabilities were estimated as a function of the plasticizer mixtures with a full cubic mixture model (Myers et al., 2009), Eq. (5):

$$y = \sum_{i=1}^{q} \beta_i x_i + \sum \sum_{i<j=2}^{q} \beta_{ij} x_i x_j + \sum \sum_{i<j=2}^{q} \delta_{ij} x_i x_j (x_i - x_j) + \beta_{ijk} x_i x_j x_k + e \quad (5)$$

where *y* denoted an observed film property, β the model coefficients, *x* the relative proportions of the plasticizers in the blend, and *e* the model residual. The model coefficients β were determined by minimizing the sum of the squares of the model residuals using the least squares estimate (Mäkelä,

2017). The statistical significance of the coefficients was evaluated by comparing the variation explained by the model term against the model residuals using an F test. Statistically insignificant ($p>0.10$) terms were then excluded from the models. The predictive ability of the models was determined with validation experiments. A combined validation error was determined as the root mean squared error (RMSE), Eq. (6):

$$RMSE = \sqrt{\frac{\sum_{i=1}^{n}(y_i - \hat{y}_i)^2}{n}} \quad (6)$$

where y and $\hat{y}$ denoted an observed and predicted film property, respectively, and n the number of validation experiments. With response transformations the predicted values were transformed back to their real units before determining the RMSE. The calculations were done with Matlab (The MathWorks Inc.) and DesignExpert (Stat-Ease Inc.) and the results were plotted in OriginPro 2024 (OriginLab Corp.).

3. Results and discussion

3.1 Technical details

We studied plasticizer blending to control the properties of regenerated cellulose films. Systematic variations in the experimental data were first determined with principal components analysis. The data are shown in Table A1 in the Appendix and the principal component loadings based on the first thirteen experiments after data normalization are shown in Fig. 1. The results showed that ultimate tensile strength and Young's modulus increased with increasing maltitol content in the plasticizer blends based on the first two principal components. Improved film strength was, however, associated with decreased strain at break. We used strain at break as an indication of film elasticity, which is an important property to prevent the film from breaking during handling and further processing. Water vapour and oxygen permeability of the films increased towards increasing glycerol in the blends (Fig. 1a). These observations indicated that the barrier properties measured from glycerol plasticized films

improved with other plasticizers. The variable correlations explained by the first and the third principal component suggested that sorbitol also contributed to increased film strength (Fig. 1b). Overall, the first three principal components explained 83% of the variation in the normalized data and provided a rough overview of the variable correlations.

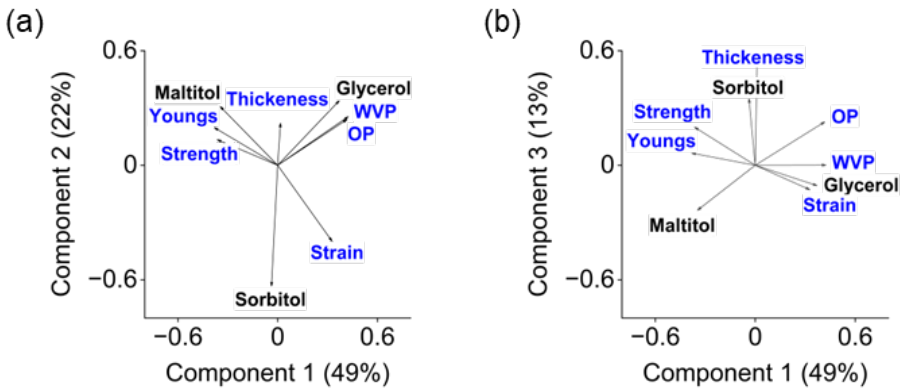

Fig. 1: Principal component loadings based on the first and the second component in (a) and the first and the third component in (b). Strength in the figure refers to ultimate tensile strength, Youngs to Young's modulus, WVP to water vapour permeability and OP to oxygen permeability.

We then used linear regression to estimate film properties based on plasticizer blend composition. We focused on tensile strength and water vapour and oxygen permeability as they are considered key indicators of film efficacy in barrier applications. Our hypothesis was that blending low molecular weight polyols with a different number of hydroxyl groups would enable us to control these properties based on blend composition. The final regression models are summarized in Table 1. The R^2 values indicated that the regression models explained 74-91% of the variation in the estimated film properties. The predictive ability of the models was evaluated with leave-one-out cross-validation. The resulting R^2_{cv} values showed that the predictions covered 49-84% of the variation in predicted film properties (Table 1). These results indicated that especially the models for ultimate tensile strength and water vapour permeability provided a good fit to the data and could potentially provide satisfactory predictions within the experimental design range. Our model for oxygen permeability

showed larger uncertainties likely due to film heterogeneity. The dissolved cellulose dopes were not filtered before casting, which could have resulted in some undissolved cellulose fractions in the final films.

Table 1: Summary of the regression models on film properties.

Film property	Unit	Transformation	Residual degrees of freedom	R^2	R^2_{cv}	RMSE[a]	Range error ratio
Ultimate tensile strength	MPa	None	9	0.91	0.73	7.1	2.2
Water vapour permeability	g·µm·m^{-2}·day^{-1}	log10	11	0.90	0.84	117.6	3.0
Oxygen permeability	cc·µm·m^{-2}·d^{-1}	log10	11	0.69	0.49	57.6	1.7

[a]Determined based on separate validation experiments. [b]Determined based on the validation results and the RMSE.

Fig. 2a shows a visualization of the experimental design. Examples of measured film properties and the measured vs. predicted film properties based on the tensile strength model are shown in Fig. 2b-2c and the corresponding results for water vapour and oxygen permeability are provided in Fig. A1. Response surfaces of the model predictions as a function of plasticizer blend composition are illustrated in Fig. 2d. Based on the results, the highest measured strength values were determined when maltitol was used as a plasticizer as suggested by the principal components (Fig. 2b). Higher

than average strength values were also determined from the ternary blends where glycerol was used as the majority component (Figs. 2b and 2d). Glycerol and sorbitol blends showed the highest strain at break values of 17% compared to the other plasticizer blends (Table A.1). Our observations on the effects of individual plasticizers were partly in line with those previously reported for cellulose nanocrystal films by Fernández-Santos et al., (2021). The authors studied the effects of individual plasticizers and plasticizer dose on film properties and reported higher strength values for maltitol than for glycerol at higher concentrations. Their cellulose nanocrystal films showed comparable elongation at break values with 10% glycerol and maltitol, but maltitol led to considerably higher elasticities when the plasticizer dose was increased to 25% (Fernández-Santos et al., 2021). These observations were not supported by our results for regenerated cellulose films which suggested that an increasing number of hydroxyl groups in the 5% plasticizer solution improved film strength but made the films more brittle. Our data, however, showed considerable variations in the strain at break values from the replicate experiments. These variations were likely generated by inconsistencies in film thickness and quality, which led to uncontrolled break during strain. Our control films showed ultimate tensile strength and strain at break values of 74 ± 8 MPa and 5 ± 2% (mean ± standard deviation, $n > 6$), respectively, whereas the films plasticized with the plasticizer blends showed on average a 12% strain at break. This indicated that plasticization generally weakened film strength and improved film elasticity as was expected.

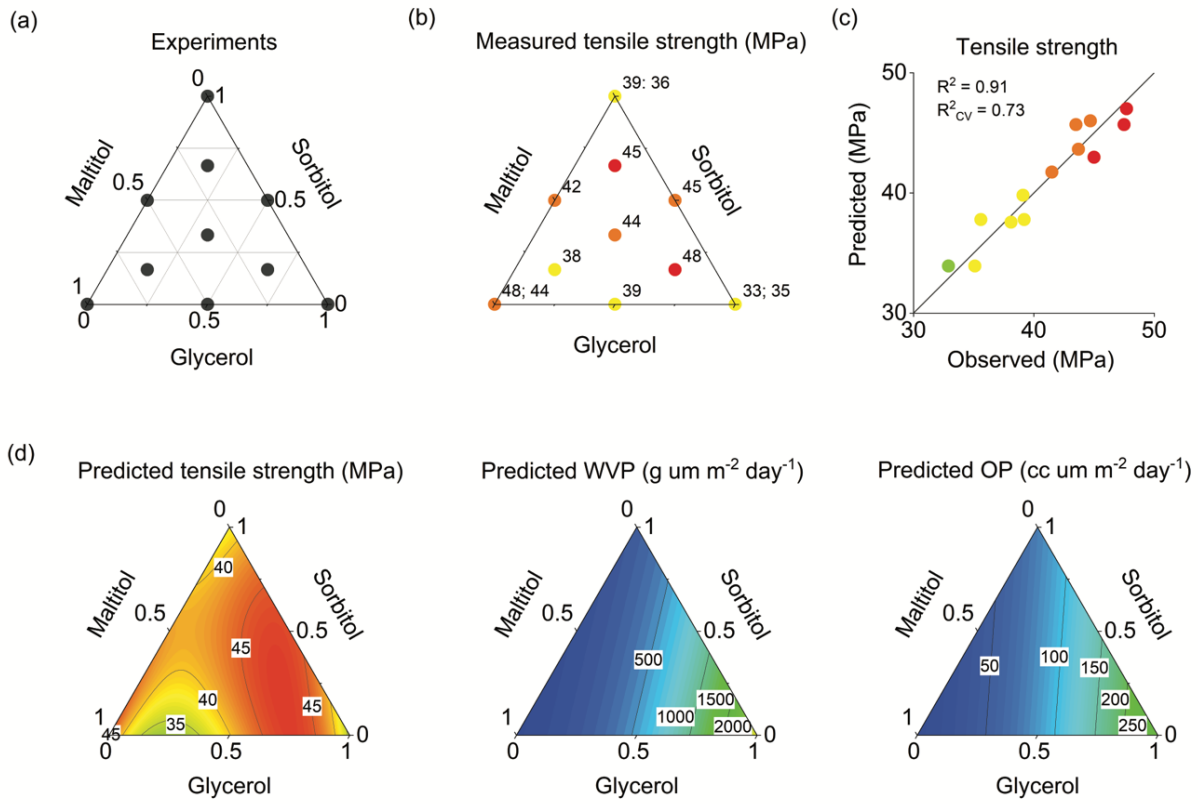

Fig. 2: A visualization of the plasticizer blend experiments in (a), measured strength values from the experiments in (b), the measured vs. predicted strength values based on the regression model in (c), and the model predictions for ultimate tensile strength, water vapour permeability (WVP), and oxygen permeability (OP) in (d).

Water vapour and oxygen permeability are key indicators of film efficacy for barrier packaging applications. Glycerol has been widely used for plasticizing cellulose films (Xiao et al. 2003) but is known to increase water vapour and oxygen permeability compared to non-plasticized films (Fernández-Santos et al., 2021; Moreira et al., 2024). The principal components showed that the barrier performance of the films deteriorated towards increasing glycerol content in the plasticizer blends (Fig. 1a). The predictions of the individual regression models for water vapour and oxygen permeability are illustrated in Fig. 2d. These results showed that the permeabilities decreased considerably with increasing sorbitol and maltitol content in the plasticizer blends. Especially maltitol was effective in improving the barrier performance of the films and decreased average measured

water vapour and oxygen permeability by 93-94% compared to the use of glycerol (Fig. A1). We also determined the water vapour and oxygen permeabilities of uncoated cellulose films produced by the viscose process at 23 °C and 50% relative humidity for comparison. These commercial films showed mean water vapor and oxygen permeabilities 2640 $g \cdot \mu m \cdot m^2 \cdot day^{-1}$ and 480 $cc \cdot \mu m \cdot m^2 \cdot day^{-1}$, respectively. These results indicated that our regenerated cellulose films had consirably better barrier properties than the uncoated cellulose films currently on the market.

Plasticizer blend composition showed a considerable effect on the barrier properties of the films. The plasticization of regenerated cellulose films is generally described through hydrogen bond formation between the hydroxyl groups of the plasticizer and those of the cellulose polymer matrix (Bonifacio et al., 2023). We hypothesized that the number of hydroxyl groups in the plasticizer might also have influenced film crystallinity (Fernández-Santos et al., 2021), which likely contributed to the barrier and tensile performance of the films (Krässig, 1993). A moist, never-dried regenerated cellulose film can be described as a swelled web of cellulose polymer chains and low molecular weight polyols can be expected to easily diffuse between these chains. At room temperature sorbitol and maltitol are both solid compounds with high crystallinity. We anticipated that this plasticizer crystallization could also be seen as an increase in the crystallinity index of the dried films. Thus, we determined the total crystallinity indices of the films with wide-angle X-ray scattering. Distinctive peaks at locations I_{110}, I_{020}, and I_{004} confirmed the cellulose II allomorph (Fig. 3a) (French, 2014), which generally forms the precipitation of dissolved cellulose (Langan et al., 2001). We did not observe distinct peaks at around 12° which are usually indicative for hydrogen bond at crystalline plane $I_{1\text{-}10}$ originating from either cellulose II or its hydrate (Kobayashi et al., 2011). We, however, observed a peak at around 28° which could be part of the crystal structure of cellulose II. We observed considerable similarities in our diffraction patterns and in those from previous studies (Ahokas et al., 2024; González Carmona et al., 2023) suggesting that the unidentified peak did not originate from the used polyols, but was likely part of cellulose II or originated from our measurement geometry.

The plasticized films showed differences in the diffraction peak intensities at approximately 20° (Fig. 3a). Thus, we used the Scherrer equation to determine crystallite size of the crystalline plane (I_{110}) of the films (French and Santiago Cintrón, 2013; Scherrer, 1918). Exact fitting of the peak I_{110} was difficult due to the overlapping peak I_{020}. The determined crystallite sizes of our model films were in the range 5.29–5.97 nm, whereas the crystallite sizes of the non-plasticized controls were 5.30 and 5.45 nm. The increase in crystallite size can be explained by the crystallization of the polyols onto the cellulose surfaces or the crystallization of the polyols themselves. Our films plasticized with 50% sorbitol and 50% maltitol showed the largest crystallite size of 6.24 nm, which can be explained with different crystallization tendencies of the polyols or possible interactions between the different polyol plasticizers.

We note that determining the crystallinity index of regenerated cellulose accurately with the Segal equation is challenging, but the method can be used to determine trends between different films (Nam et al., 2016). Yamane et al. (2006) reported that a higher planar orientation of $I_{1\text{-}10}$ and a higher crystallinity increased the density of polar hydroxyl groups on the surface of regenerated cellulose films, which resulted in higher wettability (i.e., higher hydrophilicity). Materials with high wettability tend to show higher water vapor permeability because they can absorb and transmit more polar water molecules through their structure. Our films with the highest crystallinities (Fig. 3b), however, did not result in the lowest water vapor permeabilities (Fig. 2d). Our results shown in Fig. 3b suggested that film crystallinity followed a quadratic relationship with the number of hydroxyl groups in the plasticizers ($R^2 = 0.87$, $p < 0.01$). The total crystallinity indeces for our plasticized films were in the range of 0.87–0.89, whereas the non-plasticized control films showed a total crystallinity index of 0.86. The highest crystallinities were observed with films that were plasticized with blends containing 5-8 hydroxyl groups and both crystallinity and water vapor permeability decreased when maltitol was used as the plasticizer. These observations suggested that an increase in the number of hydroxyl

groups in the plasticizer blend did not necessarily lead to an increase in the hydroxyl groups settled parallelly on the surface of the films, which would likely increase water transport.

Maltitol is a relatively complex sugar alcohol compound with 9 hydroxyl groups and a pyranose structure attached to a linear carbon chain. It has a molar mass of 344 $g \cdot mol^{-1}$ that is nearly four times higher than the molar mass of glycerol (92 $g \cdot mol^{-1}$) and nearly two times higher than the molar mass of sorbitol (192 $g \cdot mol^{-1}$). The complex and large molecule structure of maltitol may have weakened its ability to penetrate and distribute evenly between the polymer chains of the cellulose matrix (Ioelovich, 2009). Penetration of a larger molecule would likely result in higher swelling of the film (Bonifacio et al., 2023). We measured the film thicknesses (Table A1 in Appendix) but were unable to identify clear and systematic trends in thickness as a function of plasticizer composition. We measured also the film weights (Table A1 in Appendix) which showed on average a 13% weight increase in the glycerol plasticized films compared to films plasticized with maltitol. This could implicate more thorough distribution of glycerol across the film structure compared to its larger maltitol reference. Thorough understanding of the mechanisms would, however, require further studies related to distribution of the plastizers on the surface and across the film structure, and especially detailed water interaction study on film surface (e.g. with quartz crystal microbalance method).

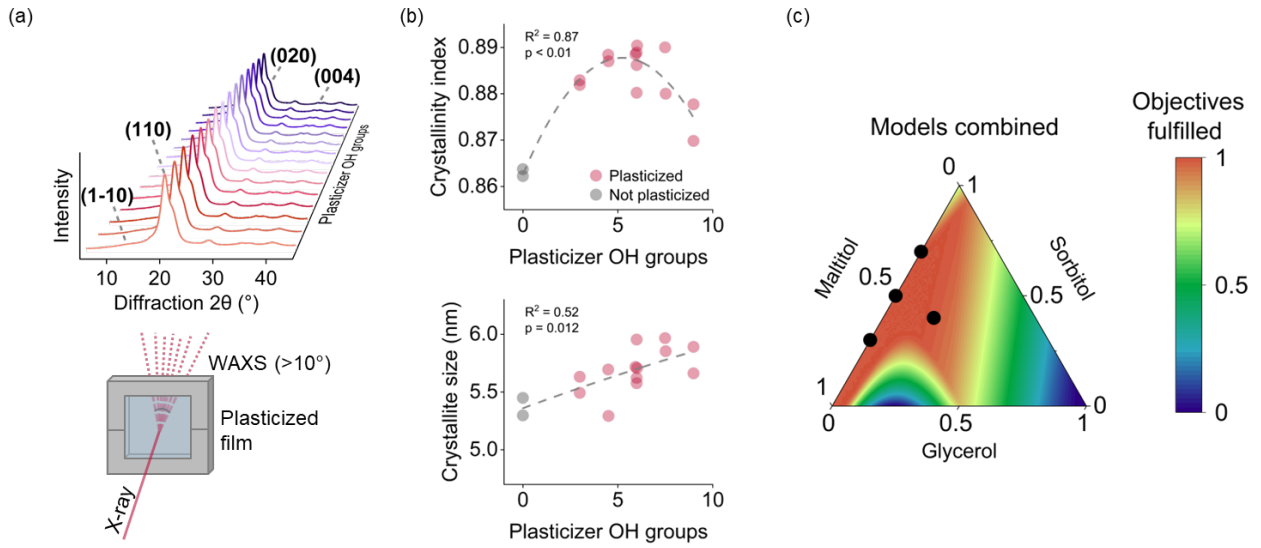

Fig. 3: Schematic illustration of the wide-angle X-ray scattering (WAXS) measurement and diffraction patterns of plasticized regenerated cellulose films in (a), crystallinity indices and crystallite sizes of the main crystalline planes (I_{110}) as a function of the hydroxyl groups in the plastificizer blends in (b), and the model predictions combined to achieve a tensile strength >40 MPa and water vapour and oxygen permeabilities <300 g·µm·m^{-2}·day^{-1} and <75 cc·µm·m^{-2}·day^{-1}, respectively, in (c). The scatter symbols in (c) show validation experiments.

Film efficacy in barrier packaging applications is affected by both mechanical and barrier properties. We combined the predictions of our individual regression models to identify promising plasticizer blend compositions for given film properties. We aimed at a tensile strength >40 MPa coupled with water vapour and oxygen permeability <300 g·µm·m^{-2}·day^{-1} and <75 cc·µm·m^{-2}·d^{-1}, respectively. The individual model predictions were first normalized to the range ([0,1]) based on these objectives and the normalized predictions were then multiplied by one another to identify plasticizer compositions where the objectives were fulfilled. The results are shown in Fig. 3c and indicated that promising plasticizer blend compositions were located in the proximity of binary sorbitol-maltitol blends. We then designed four additional validation experiments to empirically test the predictions of our regression models with these promising plasticizer blends. The validation experiments are visualized

in Fig. 3c. For example, cellulose films plasticized with 50% sorbitol and 50% maltitol showed a tensile strength of 49.7 MPa coupled with water vapour and oxygen permeabilities of 259 $g \cdot \mu m \cdot m^{-2} \cdot day^{-1}$ and 28 $cc \cdot \mu m \cdot m^{-2} \cdot d^{-1}$, respectively, which successfully met the set objectives. The rest of the validation results are given in Table A.1. The resulting RMSE values in Table 1 show the average root mean squared errors during model validation. The subsequent range error ratios suggested that the model for water vapour permeability showed in comparison the lowest validation errors followed by the models for ultimate tensile strength and oxygen permeability.

3.2 Practical considerations

Our objective was to improve regenerated cellulose films by focusing on plasticizer blending. The experimental results showed that blending simple polyols could be used to control film strength and water vapor and oxygen permeability with acceptable reliability. These findings are relevant as they indicate that plasticizer blending provides a tool to improve regenerated cellulose films, which are currently not considered as plastics in the single-use plastics directive by the European Union (European Parliament, 2019). The United Nations Environmental Assembly recently convened an Intergovernmental Negotiating Committee to develop a legally binding resolution on global plastic pollution with the aim to reduce plastic production, single-use plastics, and to promote plastic recycling (UNEP, 2022), which will further increase the demand for plastic alternatives in the future. We compared our results on the barrier properties of regenerated cellulose films and commercial cellophane against conventional petroleum-based plastics reported by Lavoine et al. (2012). The results are shown in Fig. 4 and indicate that our films matched the barrier performance of commercial cellophane and with further improvements could provide a competitive renewable alternative to polyolefin films.

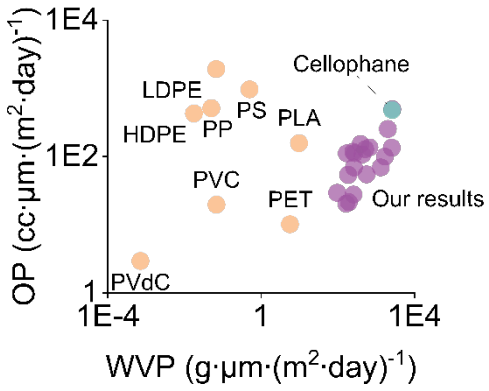

Fig. 4: Our results on the barrier performance of regenerated cellulose films and commercial cellophane compared with conventional plastics reported by Lavoine et al. (2012).

We used mechano-enzymatic pre-treatment and sodium zincate dissolution to prepare the regenerated cellulose films. This approach enables producing films without the use of hazardous carbon disulphide and the generation of sulphur-containing by-products, which are characteristic of regenerated cellulose production for viscose yarns. We, however, found no published data to assess the economics of our dissolution and precipitation approach, other than that it could be potentially installed in existing viscose production plants (Heikkilä et al., 2018). The global plastic films market size was 134.5 billion USD in 2023 and is expected to grow 31% within the next five years. We anticipate that most of the process costs associated with large-scale film production would be generated by the dissolution and film preparation steps and that the price of the polyol blends for plasticization would be comparatively lower. ChemAnalyst (2024) reported that the price of glycerol fluctuated 2-6% within 2023-2024 due to supply constraints, rising production costs of palm oil, and geopolitical tensions. By the end of 2024, glycerol prices settled to 383-943 USD per metric tonne in Shanghai, Saudi-Arabia, and South Korea (ChemAnalyst, 2024b). By the end of the quarter 2024, 70% sorbitol cost 731-1340 USD per metric tonne in New York, China and France (ChemAnalyst, 2024c). Our findings on plasticizer blending could potentially be applied also to other dissolution and precipitation chemistries. For example, N-methylmorpholine N-oxide dissolution is already in commercial use in the production of lyocell fibers for textiles and has shown acceptable chemical

recovery rates and profitability when raw material and capital costs are reasonable (Hytönen et al., 2023). Overall, we foresee an increasing future demand for renewable and competitive alternatives to conventional plastics based on existing European Union regulations and the recent United Nations initiative.

Conclusions

We studied the effects of glycerol, sorbitol, and maltitol on the properties of regenerated cellulose films based on plasticizer blending. Our results showed that blending the three polyols enabled us to control film strength and water vapour and oxygen permeability, which are key indicators to evaluate film efficacy in barrier packaging applications. Plasticizer blending thus provides a novel and simple approach to improve the mechanical and barrier properties of regenerated cellulose films as an alternative to plastics in applications where higher elasticity is required. The barrier performance of our plasticized films was better than commercial uncoated cellophane film and could potentially provide a renewable alternative to fossil-based polyolefin films with further improvements. These findings are important to combat the low recycling rates of conventional plastic films in packaging applications and to adapt to the current European Union regulations and the United Nations initiative to improve plastic recycling, to reduce single-use plastics, and to reduce overall plastics production. Plasticization of the regenerated cellulose films will greatly benefit from property prediction with regression models towards targeted applications. We foresee an increasing future demand for renewable and competitive alternatives for conventional plastics in packaging and other applications.

Author contributions

Pauliina Ahokas: Data curation, Formal analysis, Validation, Visualization, Writing – original draft, Writing – review and editing. **Vesa Kunnari:** Conceptualization, Project administration, Resources, Supervision, Writing – review and editing. **Johanna Majoinen:** Project administration, Resources, Supervision, Writing – review and editing. **Ali Harlin:** Funding acquisition, Supervision, Writing – review and editing. **Mikko Mäkelä:** Conceptualization, Data curation, Formal analysis, Methodology, Software, Validation, Visualization, Writing – original draft, Writing – review and editing.

Conflicts of interest

The authors declare no conflicts of interest.

Acknowledgements

This work was financially supported by the European Regional Development Fund and the participating companies through the project A80423 F3 - Films or future. We gratefully acknowledge Vuokko Liukkonen, Katja Pettersson, Ulla Salonen, and Maritta Räsänen from VTT Technical Research Centre of Finland Ltd. for preparing and analyzing the films.

References

Ahokas, P., Mäkelä, M., Jaiswal, A., Khakalo, A., Harlin, A., 2024. Controlling the rheology of cellulose dissolved in 4 – methylmorpholine N – oxide and tensile properties of precipitated cellulose films via mixture design. Cellulose. https://doi.org/10.1007/s10570-024-06214-y

Azubuike, C.P., Rodríguez, H., Okhamafe, A.O., Rogers, R.D., 2012. Physicochemical properties of maize cob cellulose powders reconstituted from ionic liquid solution. Cellulose 19, 425–433. https://doi.org/10.1007/s10570-011-9631-y

Bonifacio, A., Bonetti, L., Piantanida, E., De Nardo, L., 2023. Plasticizer Design Strategies Enabling Advanced Applications of Cellulose Acetate. Eur. Polym. J. 197, 112360. https://doi.org/10.1016/j.eurpolymj.2023.112360

Bro, R., Smilde, A.K., 2014. Principal component analysis. Anal. Methods 6, 2812–2831. https://doi.org/10.1039/c3ay41907j

Cazón, P., Velázquez, G., Vázquez, M., 2020. Regenerated cellulose films combined with glycerol and polyvinyl alcohol: Effect of moisture content on the physical properties. Food Hydrocoll.

103. https://doi.org/10.1016/j.foodhyd.2020.105657

ChemAnalyst, 2024a. Polyol Price Trend and Forecast [WWW Document]. Chem. Prices. URL https://www.chemanalyst.com/Pricing-data/polyols-60 (accessed 11.26.24).

ChemAnalyst, 2024b. Glycerine Price Trend and Forecast [WWW Document]. Chem. Prices. URL https://www.chemanalyst.com/Pricing-data/glycerine-1168 (accessed 11.28.24).

ChemAnalyst, 2024c. Sorbitol Price Trend and Forecast [WWW Document]. Chem. Prices. URL https://www.chemanalyst.com/Pricing-data/sorbitol-1274 (accessed 12.16.24).

de Britto, D., de Rizzo, J.S., Assis, O.B.G., 2012. Effect of Carboxymethylcellulose and Plasticizer Concentration on Wetting and Mechanical Properties of Cashew Tree Gum-Based Films. Int. J. Polym. Anal. Charact. 17, 302–311. https://doi.org/10.1080/1023666X.2012.668449

de Mello Soares, C.T., Ek, M., Östmark, E., Gällstedt, M., Karlsson, S., 2022. Recycling of multi-material multilayer plastic packaging: Current trends and future scenarios. Resour. Conserv. Recycl. 176. https://doi.org/10.1016/j.resconrec.2021.105905

European Parliament, 2019. The reduction of the impact of certain plastic products on the environment. European Union.

Fernández-Santos, J., Valls, C., Cusola, O., Roncero, M.B., 2021. Improving Filmogenic and Barrier Properties of Nanocellulose Films by Addition of Biodegradable Plasticizers. ACS Sustain. Chem. Eng. 9, 9647–9660. https://doi.org/10.1021/acssuschemeng.0c09109

French, A.D., 2014. Idealized powder diffraction patterns for cellulose polymorphs. Cellulose 21, 885–896. https://doi.org/10.1007/s10570-013-0030-4

French, A.D., Santiago Cintrón, M., 2013. Cellulose polymorphy, crystallite size, and the Segal

Crystallinity Index. Cellulose 20, 583–588. https://doi.org/10.1007/s10570-012-9833-y

Geyer, R., Jambeck, J.R., Law, K.L., 2017. Production, use, and fate of all plastics ever made. Sci. Adv. 3, 25–29. https://doi.org/10.1126/sciadv.1700782

González Carmona, E., Schlapp-Hackl, I., Jääskeläinen, S., Järvinen, M., Nieminen, K., Sawada, D., Hummel, M., Sixta, H., 2023. Development of cellulose films by means of the Ioncell® technology, as an alternative to commercial films. Cellulose 30, 11633–11648. https://doi.org/10.1007/s10570-023-05588-9

Grönqvist, S., Hakala, T.K., Kamppuri, T., Vehviläinen, M., Hänninen, T., Liitiä, T., Maloney, T., Suurnäkki, A., 2014. Fibre porosity development of dissolving pulp during mechanical and enzymatic processing. Cellulose 21, 3667–3676. https://doi.org/10.1007/s10570-014-0352-x

Grönqvist, S., Kamppuri, T., Maloney, T., Vehviläinen, M., Liitiä, T., Suurnäkki, A., 2015. Enhanced pre-treatment of cellulose pulp prior to dissolution into NaOH/ZnO. Cellulose 22, 3981–3990. https://doi.org/10.1007/s10570-015-0742-8

Heikkilä, P., Fontell, P., Kamppuri, T., Mensonen, A., Määttänen, M., Pitkänen, M., Raudaskoski, A., Vehmas, K., Vehviläinen, M., Harlin, A., 2018. The Relooping Fashion Initiative. VTT Res. Rep. No. VTT-R-01703-18 36.

Hirvikorpi, T., Vähä-Nissi, M., Mustonen, T., Iiskola, E., Karppinen, M., 2010. Atomic layer deposited aluminum oxide barrier coatings for packaging materials. Thin Solid Films 518, 2654–2658. https://doi.org/10.1016/j.tsf.2009.08.025

Hytönen, E., Sorsamäki, L., Kolehmainen, E., Sturm, M., von Weymarn, N., 2023. Lyocell fibre production using NMMO – A simulation-based techno-economic analysis. BioResources 18, 6384–6411. https://doi.org/10.15376/biores.18.3.6384-6411

Ioelovich, M., 2009. Accessibility and crystallinity of cellulose. BioResources 4, 1168–1177. https://doi.org/10.15376/biores.4.3.1168-1177

Jin, Z., Wang, S., Wang, J., Zhao, M., 2011. Effects of Plasticization Conditions on the Structures and Properties of Cellulose Packaging Films from Ionic Liquid [BMIM]Cl. J. Appl. Polym. Sci. 125, 704–709.

Klemm, D., Heublein, B., Fink, H.-P., Bohn, A., 2005. Cellulose: Fascinating Biopolymer and Sustainable Raw Material. Angew. Chemie Int. Ed. 44, 3358–3393. https://doi.org/10.1002/anie.200460587

Kobayashi, K., Kimura, S., Togawa, E., Wada, M., 2011. Crystal transition from cellulose II hydrate to cellulose II. Carbohydr. Polym. 86, 975–981. https://doi.org/10.1016/j.carbpol.2011.05.050

Kolpak, F.J., Blackwell, J., 1976. Determination of the Structure of Cellulose II. Macromolecules 9, 273–278. https://doi.org/10.1021/ma60050a019

Krässig, H.A., 1993. 4. Structure and Physico-Chemical Properties, in: Huglin, M.B. (Ed.), Cellulose: Structure, Accessibility and Reactivity. Gordon and Breach Science Publishers, Yverdon, pp. 150–166.

Langan, P., Nishiyama, Y., Chanzy, H., 2001. X-ray structure of mercerized cellulose II at 1 Å resolution. Biomacromolecules 2, 410–416. https://doi.org/10.1021/bm005612q

Lavoine, N., Desloges, I., Dufresne, A., Bras, J., 2012. Microfibrillated cellulose - Its barrier properties and applications in cellulosic materials: A review. Carbohydr. Polym. 90, 735–764. https://doi.org/10.1016/j.carbpol.2012.05.026

Lee, K.J., Choi, K., 2024. Environmental occurrence, human exposure, and endocrine disruption of

di-iso-nonyl phthalate and di-iso-decyl phthalate: A systematic review. Crit. Rev. Environ. Sci. Technol. 54, 603–640. https://doi.org/10.1080/10643389.2023.2261815

Mäkelä, M., 2017. Experimental design and response surface methodology in energy applications: A tutorial review. Energy Convers. Manag. 151, 630–640. https://doi.org/10.1016/j.enconman.2017.09.021

Mokwena, K.K., Tang, J., 2012. Ethylene Vinyl Alcohol: A Review of Barrier Properties for Packaging Shelf Stable Foods. Crit. Rev. Food Sci. Nutr. 52, 640–650. https://doi.org/10.1080/10408398.2010.504903

Moreira, R., Rebelo, R.C., Coelho, J.F.J., Serra, A.C., 2024. Novel thermally regenerated flexible cellulose-based films. Eur. J. Wood Wood Prod. https://doi.org/10.1007/s00107-024-02126-7

Myers, R.H., Montgomery, D.C., Anderson-Cook, C.M., 2009. Response surface methodology - process and product optimisation using designed experiments, in: Wiley Series in Probability and Statistics. John Wiley & Sons, Inc.

Nam, S., French, A.D., Condon, B.D., Concha, M., 2016. Segal crystallinity index revisited by the simulation of X-ray diffraction patterns of cotton cellulose Iβ and cellulose II. Carbohydr. Polym. 135, 1–9. https://doi.org/10.1016/j.carbpol.2015.08.035

OECD, 2024a. Global Plastics Outlook: Plastics use by application [WWW Document]. OECD Environ. Stat. https://doi.org/10.1787/234a9f22-en

OECD, 2024b. Global Plastics Outlook: Plastic waste in 2019 [WWW Document]. OECD Environ. Stat. https://doi.org/10.1787/a92f5ea3-en

OECD, 2024c. Global Plastics Outlook: Plastic waste by end-of-life fate - projections [WWW Document]. OECD Environ. Stat. https://doi.org/10.1787/3f85b1c2-en

Park, S., Baker, J.O., Himmel, M.E., Parilla, P.A., Johnson, D.K., 2010. Cellulose crystallinity index: measurement techniques and their impact on interpreting cellulase performance. Biotechnol. Biofuels 3, 1–14. https://doi.org/10.1186/1754-6834-3-10

Peng, J., Li, Y., Liu, X., Ke, G., Song, D., Wu, S., Xu, W., Zhu, K., 2021. Cellulose film with air barrier and moisture-conducting character fabricated by NMMO. J. Mater. Sci. 56, 18313–18326. https://doi.org/10.1007/s10853-021-06499-5

Ragaert, K., Delva, L., Van Geem, K., 2017. Mechanical and chemical recycling of solid plastic waste. Waste Manag. 69, 24–58. https://doi.org/10.1016/j.wasman.2017.07.044

Ragonnaud, G., 2023. EU Legislation in Progress - Revision of the Packaging and Packaging Waste Directive. Eur. Parliam. Res. Serv. .

Rebelo, R.C., Ribeiro, D.C.M., Pereira, P., De Bon, F., Coelho, J.F.J., Serra, A.C., 2023. Cellulose-based films with internal plasticization with epoxidized soybean oil. Cellulose 30, 1823–1840. https://doi.org/10.1007/s10570-022-04997-6

Sanyang, M.L., Sapuan, S.M., Jawaid, M., Ishak, M.R., Sahari, J., 2015. Effect of plasticizer type and concentration on tensile, thermal and barrier properties of biodegradable films based on sugar palm (Arenga pinnata) starch. Polymers (Basel). 7, 1106–1124. https://doi.org/10.3390/polym7061106

Scheffe, H., 1963. The Simplex-Centroid Design for Experiments with Mixtures. J. R. Stat. Soc. Ser. B 25, 235–63. https://doi.org/10.1111/j.2517-6161.1963.tb00506.x

Scherrer, P., 1918. Bestimmung der Größe und der inneren Struktur von Kolloidteilchen mittels Röntgenstrahlen. Nachrichten von der Gesellschaft der Wissenschaften zu Göttingen, Math. Klasse 1918, 98–100.

Segal, L., Creely, J.J., Martin, A.E., Conrad, C.M., 1959. An Empirical Method for Estimating the Degree of Crystallinity of Native Cellulose Using the X-Ray Diffractometer. Text. Res. J. 29, 786–794. https://doi.org/10.1177/004051755902901003

Singh, P., Duarte, H., Alves, L., Antunes, F., Le Moigne, N., Dormanns, J., Duchemin, B., Staiger, M.P., Medronho, B., 2015. From Cellulose Dissolution and Regeneration to Added Value Applications — Synergism Between Molecular Understanding and Material Development, in: Poletto, M., Ornaghi, H.L.J. (Eds.), Cellulose - Fundamental Aspects and Current Trends. IntechOpen, pp. 1–45.

Struller, C.F., Kelly, P.J., Copeland, N.J., 2014. Aluminum oxide barrier coatings on polymer films for food packaging applications. Surf. Coatings Technol. 241, 130–137. https://doi.org/10.1016/j.surfcoat.2013.08.011

UNEP, 2022. Resolution 5/14. End plastic pollution: Towards an international legally binding instrument. United Nations Environ. Program. 1–6.

Vehviläinen, M., Kamppuri, T., Grönqvist, S., Rissanen, M., Maloney, T., Honkanen, M., Nousiainen, P., 2015. Dissolution of enzyme-treated cellulose using freezing–thawing method and the properties of fibres regenerated from the solution. Cellulose 22, 1653–1674. https://doi.org/10.1007/s10570-015-0632-0

Vehviläinen, M., Määttänen, M., Grönqvist, S., Harlin, A., Steiner, M., Kunkel, R., 2020. Sustainable continuous process for cellulosic regenerated fibers. Chem. Fibers Int. 70, 128–130.

Vessa, B., Perlman, B., McGovern, P.G., Morelli, S.S., 2022. Endocrine disruptors and female fertility: a review of pesticide and plasticizer effects. F S Reports 3, 86–90. https://doi.org/10.1016/j.xfre.2022.04.003

Xiao, C., Zhang, Z., Zhang, J., Lu, Y., Zhang, L., 2003. Properties of regenerated cellulose films plasticized with α-monoglycerides. J. Appl. Polym. Sci. 89, 3500–3505. https://doi.org/10.1002/app.12509

Yamane, C., Aoyagi, T., Ago, M., Sato, K., Okajima, K., Takahashi, T., 2006. Two different surface properties of regenerated cellulose due to structural anisotropy. Polym. J. 38, 819–826. https://doi.org/10.1295/polymj.PJ2005187

Zhang, Y. qing, Li, J., Huang, X. juan, Yang, C. xia, Wu, C., Yang, Z. lei, Li, D. qiang, 2023. Performance-enhanced regenerated cellulose film by adding grape seed extract. Int. J. Biol. Macromol. 232, 123290. https://doi.org/10.1016/j.ijbiomac.2023.123290